

Effects of carrier density and interactions on pairing symmetry in a t_{2g} model

Yun-Xiao Li(李云霄), Wen-Han Xi(西文翰), Zhao-Yang Dong(董召阳), Zi-Jian Yao(姚子健), Shun-Li Yu(于顺利), and Jian-Xin Li(李建新)

Citation: Chin. Phys. B, 2024, 33 (**1**): 017404. DOI: 10.1088/1674-1056/ad1094

Journal homepage: http://cpb.iphy.ac.cn; http://iopscience.iop.org/cpb

What follows is a list of articles you may be interested in

Pressure tuning of the anomalous Hall effect in the kagome superconductor CsV_3Sb_5

Fang-Hang Yu(喻芳航), Xi-Kai Wen(温茜凯), Zhi-Gang Gui(桂智刚), Tao Wu(吴涛), Zhenyu Wang(王震宇), Zi-Ji Xiang(项子雾), Jianjun Ying(应剑俊), and Xianhui Chen(陈仙辉)

Chin. Phys. B, 2022, 31 (**1**): 017405. DOI: 10.1088/1674-1056/ac3990

A review of some new perspectives on the theory of superconducting Sr_2RuO_4

Wen Huang(黄文)

Chin. Phys. B, 2021, 30 (**10**): 107403. DOI: 10.1088/1674-1056/ac2488

Superconductivity in twisted multilayer graphene: A smoking gun in recent condensed matter physics

Yonghuan Chu(楚永唤), Fangduo Zhu(朱方铎), Lingzhi Wen(温凌志), Wanying Chen(陈婉莹), Qiaoni Chen(陈巧妮), and Tianxing Ma(马天星)

Chin. Phys. B, 2020, 29 (**11**): 117401. DOI: 10.1088/1674-1056/abbbea

Superconductivity with peculiar upper critical fields in quasi-one-dimensional Cr-based pnictides

Guang-Han Cao(曹光旱), Zeng-Wei Zhu(朱增伟)

Chin. Phys. B, 2018, 27 (**10**): 107401. DOI: 10.1088/1674-1056/27/10/107401

Quantum critical behavior in an antiferromagnetic heavy-fermion Kondo lattice system $(Ce_{1-x}La_x)_2Ir_3Ge_5$

Rajwali Khan, Qianhui Mao(毛乾辉), Hangdong Wang(王杭栋), Jinhu Yang(杨金虎), Jianhua Du(杜建华), Binjie Xu(许彬杰), Yuxing Zhou(周宇星), Yannan Zhang(张燕楠), Bing Chen(陈斌), Minghu Fang(方明虎)

Chin. Phys. B, 2017, 26 (**1**): 017401. DOI: 10.1088/1674-1056/26/1/017401

RAPID COMMUNICATION

Effects of carrier density and interactions on pairing symmetry in a t_{2g} model

Yun-Xiao Li(李云霄)[1], Wen-Han Xi(西文翰)[1], Zhao-Yang Dong(董召阳)[2], Zi-Jian Yao(姚子健)[3], Shun-Li Yu(于顺利)[1,4,†], and Jian-Xin Li(李建新)[1,4,‡]

[1] *National Laboratory of Solid State Microstructures and Department of Physics, Nanjing University, Nanjing* 210093, *China*
[2] *Nanjing University of Science and Technology, Nanjing* 210094, *China*
[3] *Department of Physics, Nanjing Normal University, Nanjing* 210023, *China*
[4] *Collaborative Innovation Center of Advanced Microstructures, Nanjing University, Nanjing* 210093, *China*

(Received 21 October 2023; revised manuscript received 16 November 2023; accepted manuscript online 29 November 2023)

By utilizing the fluctuation exchange approximation method, we perform a study on the superconducting pairing symmetry in a t_{2g} three-orbital model on the square lattice. Although the tight-binding parameters of the model are based on Sr_2RuO_4, we have systematically studied the evolution of superconducting pairing symmetry with the carrier density and interactions, making our findings relevant to a broader range of material systems. Under a moderate Hund's coupling, we find that spin fluctuations dominate the superconducting pairing, leading to a prevalent spin-singlet pairing with a $d_{x^2-y^2}$-wave symmetry for the carrier density within the range of $n = 1.5$–4 per site. By reducing the Hund's coupling, the charge fluctuations are enhanced and play a crucial role in determining the pairing symmetry, leading to a transition of the pairing symmetry from the spin-singlet $d_{x^2-y^2}$-wave to the spin-triplet p-wave. Furthermore, we find that the superconducting pairings are orbital dependent. As the carrier density changes from $n = 4$ to $n = 1.5$, the active orbitals for superconducting pairing shift from the quasi-two-dimensional orbital d_{xy} to the quasi-one-dimensional orbitals d_{xz} and d_{yz}.

Keywords: unconventional superconductivity, pairing mechanism, Fermi surface, three-orbital model

PACS: 74.20.–z, 74.20.Rp, 71.18.+y, 75.10.Lp **DOI:** 10.1088/1674-1056/ad1094

1. Introduction

In recent years, there has been a growing interest in the study of unconventional superconductivity (SC) in multi-orbital systems, including Fe-based superconductors,[1–7] Sr_2RuO_4,[8–14] vanadium-based kagome superconductors,[15–24] and Ni-based superconducting materials.[25–31] In these superconductors, the low-energy physical properties are mainly determined by the d-orbital electrons of the transition metal atoms. In real materials, the five d orbitals in these materials are no longer degenerate due to the tetrahedral or octahedral crystal fields, resulting in the triple-degenerate t_{2g} orbitals and the double-degenerate e_g orbitals. In a tetrahedral crystal field, as is the case of iron-based superconductors, the energy of the t_{2g} orbitals is higher than that of the e_g orbitals. Conversely, in an octahedral crystal field, such as in Sr_2RuO_4, the energy of the e_g orbitals is higher than that of the t_{2g} orbitals. As a result, for materials with a tetrahedral lattice structure, the low-energy physical properties are mainly governed by the t_{2g} orbitals when the number of d electrons exceeds 4 per lattice site, such as in the iron-based superconductors. Similarly, for materials with an octahedral lattice structure, the low-energy physical properties are also dominated by the t_{2g} orbitals when the number of d electrons is less than 6 per lattice site, such as in Sr_2RuO_4. Therefore, a systematic study of the superconducting pairing symmetry in the t_{2g} three-orbital models is important for understanding the superconducting mechanism of the superconductors dominated by electrons in d-orbitals. Moreover, the t_{2g} orbitals also play a vital role in determining the low-energy physics of many magnetic materials, such as Na_2IrO_3[32–37] and α-$RuCl_3$,[38–46] which have gained considerable attention in recent years. The realization of superconductivity in these materials through doping is also a subject of interest in current experimental research. Thus, a systematic investigation of the superconducting pairing symmetry with respect to the doping levels and Coulomb interactions in the t_{2g} three-orbital models can also provide valuable theoretical references for exploring new novel superconducting materials.

Many d-orbital superconducting materials exhibit a quasi-two-dimensional lattice structure. Due to the strong directionality of the t_{2g} (d_{xy}, d_{xz} and d_{yz}) orbitals, the hopping integrals of these orbitals are anisotropic within the two-dimensional plane. For instance, in Sr_2RuO_4,[47] the d_{xz} and d_{yz} orbitals have highly anisotropic hopping integrals, approaching zero for d_{xz} in the y direction and d_{yz} in the x direction, which gives rise to quasi-one-dimensional properties. By contrast, the iron-based superconductors lack such strong anisotropy

†Corresponding author. E-mail: slyu@nju.edu.cn
‡Corresponding author. E-mail: jxli@nju.edu.cn

© 2024 Chinese Physical Society and IOP Publishing Ltd

in the d_{xz} and d_{yz} hopping integrals, exhibiting quasi-two-dimensional properties. Consequently, t_{2g} three-orbital models can be divided into two groups based on the quasi-one-dimensional or quasi-two-dimensional characteristics of the d_{xz} and d_{yz} orbitals. The superconducting pairing symmetry of the latter group has been extensively studied across a broad range of doping levels (from electron to hole doping) in the context of iron-based superconductivity.[48–54] In contrast, the evolution of superconducting pairing symmetry with electron concentrations in the former group has not been explored, as Sr_2RuO_4 only involves a fixed electron concentration. Investigating the electron-density dependence of the pairing symmetry in the related model will help supplement our understanding of the superconducting mechanism in the d-orbital systems.

In this paper, we employ the fluctuation exchange approximation (FLEX) method to perform a comprehensive and systematic investigation of the evolution of superconducting pairing symmetry with respect to the carrier density and interaction parameters in the t_{2g} three-orbital model, where the d_{xz} and d_{yz} orbitals exhibit quasi-one-dimensional characteristics. Despite the tight-binding parameters of the model being based on Sr_2RuO_4, our study systematically explores the influence of carrier density and interactions on the evolution of superconducting pairing symmetry, which makes our findings applicable to a wider range of material systems. When the Hund's coupling J is at a moderate level relative to the Hubbard interaction U (around $J = 0.25U$), the superconducting pairing symmetry is mainly mediated by spin fluctuations and the system shows a strong preference for the spin-singlet pairing with a $d_{x^2-y^2}$-wave throughout the entire particle concentration range we considered ($n = 1.5$–4 per site). Furthermore, we find that a decrease in J leads to an enhancement of the charge fluctuations, resulting in a transition of the most favorable superconducting pairing symmetry from spin-singlet $d_{x^2-y^2}$-wave to spin-triplet p-wave. We find that the superconducting pairings are orbital dependent. As the particle concentration changes from $n = 4$ to $n = 1.5$, the active orbitals for superconducting pairing shift from the quasi-two-dimensional orbital d_{xy} to the quasi-one-dimensional orbitals d_{xz} and d_{yz}. Our studies uncover detail evolutions of the superconducting pairing symmetries in the t_{2g} three-orbital model, and provide an insight to understand and explore the related material systems.

The paper is organized as follows. Section 2 introduces the three-orbital Hubbard model and the FLEX method. Section 3 presents the theoretical results and discussions. Finally, Section 4 provides the summary.

2. Model and method

The Hamiltonian of the t_{2g} three-orbital Hubbard model is given by

$$\begin{aligned} H = & \sum_{\boldsymbol{k},a,b,\sigma} \varepsilon_{\boldsymbol{k}}^{ab} c_{\boldsymbol{k}a\sigma}^{\dagger} c_{\boldsymbol{k}b\sigma} + \frac{U}{2} \sum_{i,a,\sigma\neq\sigma'} n_{ia\sigma} n_{ia\sigma'} \\ & + \frac{U'}{2} \sum_{i,a\neq b,\sigma,\sigma'} n_{ia\sigma} n_{ib\sigma'} + \frac{J}{2} \sum_{i,a\neq b,\sigma\neq\sigma'} c_{ia\sigma}^{\dagger} c_{ib\sigma'}^{\dagger} c_{ia\sigma'} c_{ib\sigma} \\ & + \frac{J'}{2} \sum_{i,a\neq b,\sigma\neq\sigma'} c_{ia\sigma}^{\dagger} c_{ia\sigma'}^{\dagger} c_{ib\sigma'} c_{ib\sigma}. \end{aligned} \tag{1}$$

Here, $\boldsymbol{k}$, σ and i denote the momentum, spin and lattice site, respectively. Labels a and b represent the three t_{2g} orbitals (d_{xy}, d_{xz} and d_{yz}). $c_{\boldsymbol{k}a\sigma}^{\dagger}$ ($c_{\boldsymbol{k}a\sigma}$) is the electronic creation (annihilation) operator, and $n_{ia\sigma} = c_{ia\sigma}^{\dagger} c_{ia\sigma}$ is the particle number operator. We consider the nearest-neighbor and the next-nearest-neighbor hoppings on a square lattice, and correspondingly the tight-binding dispersions $\varepsilon_{\boldsymbol{k}}$ are $\varepsilon_{\boldsymbol{k}}^{11} = -2t_1(\cos k_x + \cos k_y) - 4t_2 \cos k_x \cos k_y - \Delta - \mu_0$, $\varepsilon_{\boldsymbol{k}}^{22} = -2t_3 \cos k_x - 2t_4 \cos k_y - \mu_0$, $\varepsilon_{\boldsymbol{k}}^{33} = -2t_3 \cos k_y - 2t_4 \cos k_x - \mu_0$ and $\varepsilon_{\boldsymbol{k}}^{23/32} = -4\lambda \sin k_x \sin k_y$, where 1, 2 and 3 represent the d_{xy}, d_{xz} and d_{yz} orbitals, respectively. Here, Δ is the difference in on-site energy between d_{xy} and other two orbitals, and μ_0 is the chemical potential determined by the total particle number. Similar to Sr_2RuO_4, the tight-binding parameters in hopping matrix are set as $(t_1, t_2, t_3, t_4, \lambda, \Delta, \mu_0) = (1.0, 0.395, 1.25, 0.125, 0.1, 0.2, 1.35)$ and the resulting band structure is shown in Fig. 1(a). The α and β bands come from the hybridization of d_{xz} and d_{yz} orbitals, while the γ band consists solely of the d_{xy} orbital. The local interaction parameters include the intraorbital Coulomb interaction (U), interorbital Coulomb interaction (U'), Hund's coupling (J), and interorbital pairing hopping (J').[55] In the following calculations, we use the relationship $J = J'$ and $U = U' + 2J$ between the interaction parameters.

We carry out the investigation of the superconducting pairing symmetry by using the FLEX method[49,56–63] which is a self-consistent conserving approximation that is well-suited to the scenario of superconductivity mediated by spin and charge fluctuations. Since we adopt the three-orbital model, all the physical quantities below are matrices.[57] The renormalized Green's function $G(k)$ is obtained from the Dyson equation

$$G(k)^{-1} = G^{(0)}(k)^{-1} - \Sigma(k), \tag{2}$$

where the bare Green's function $G^{(0)}(k)^{-1}$ is

$$G^{(0)}(k) = [\mathrm{i}\omega_n + \mu - \varepsilon_{\boldsymbol{k}}]^{-1} \tag{3}$$

and the self-energy $\Sigma(k)$ is given by

$$\Sigma_{mn}(k) = \frac{T}{N} \sum_{q} \sum_{\mu\nu} V_{n\mu,m\nu}(q) G_{\mu\nu}(k-q). \tag{4}$$

Under the FLEX approximation, the effective interaction $V_{n\mu,m\nu}$ is expressed as

$$V_{n\mu,m\nu}(q) = \left\{\frac{3}{2}U^{\rm s}[(1-\chi^0(q)U^{\rm s})^{-1}-1]\chi^0(q)U^{\rm s} + \frac{1}{2}U^{\rm c}[(1+\chi^0(q)U^{\rm c})^{-1}-1]\chi^0(q)U^{\rm c} + \frac{1}{2}(U^{\rm s}\chi^0(q)U^{\rm s}+U^{\rm c}\chi^0(q)U^{\rm c})\right\}_{n\mu,m\nu}, \quad (5)$$

where $U^{\rm s}$ and $U^{\rm c}$ represent the interaction vertices of the spin and charge fluctuations, respectively. The elements of $U^{\rm s}$ ($U^{\rm c}$) are given as follows: for $i=j=k=l$, $U^{\rm s}_{ij,kl}=U$ ($U^{\rm c}_{ij,kl}=U$); for $i=j\neq k=l$, $U^{\rm s}_{ij,kl}=J$ ($U^{\rm c}_{ij,kl}=2U'-J$); for $i=k$, $j=l$ and $i\neq j$, $U^{\rm s}_{ij,kl}=U'$ ($U^{\rm c}_{ij,kl}=-U'+2J$); for $i=l$, $j=k$ and $i\neq j$, $U^{\rm s}_{ij,kl}=J$ ($U^{\rm c}_{ij,kl}=J$); for other cases, $U^{\rm s}_{ij,kl}=0$ ($U^{\rm c}_{ij,kl}=0$). The irreducible susceptibility is

$$\chi^0_{n\mu,m\nu}(q) = -\frac{T}{N}\sum_k G_{mn}(k+q)G_{\mu\nu}(k), \quad (6)$$

and correspondingly the spin and susceptibility are

$$\chi^{\rm s}(q) = [1-\chi^0(q)U^{\rm s}]^{-1}\chi^0(q), \quad (7)$$

$$\chi^{\rm c}(q) = [1+\chi^0(q)U^{\rm s}]^{-1}\chi^0(q). \quad (8)$$

The electron density is determined by $n=\frac{T}{N}\sum_k {\rm e}^{{\rm i}\omega_n 0^+}{\rm Tr}G(k)$. In the above equations, $k\equiv(\boldsymbol{k},{\rm i}\omega_n)$ and $q\equiv(\boldsymbol{q},{\rm i}\nu_n)$ are used, where $\omega_n=(2n+1)\pi T$ and $\nu_n=2n\pi T$ denote the Matsubara frequencies for fermions and bosons, respectively. In the following calculations, we will use 32×32 meshes in the momentum space, 8192 Matsubara frequencies and $T=0.01$.

After obtaining the renormalized Green's function through a self-consistent solution of Eqs. (2)–(8), the superconducting pairing functions are determined by solving the Eliashberg equation

$$\lambda\psi_{mn}(k) = -\frac{T}{N}\sum_q\sum_{\alpha\beta}\sum_{\mu\nu}V^{\rm sing,trip}_{\alpha m,n\beta}(q)G_{\alpha\mu}(k-q) \times G_{\beta\nu}(q-k)\psi_{\mu\nu}(k-q), \quad (9)$$

where the effective pairing interactions in the spin-singlet and spin-triplet channels respectively are

$$V^{\rm sing}(q) = \frac{3}{2}U^{\rm s}\chi^{\rm s}(q)U^{\rm s}-\frac{1}{2}U^{\rm c}\chi^{\rm c}(q)U^{\rm c}+\frac{1}{2}(U^{\rm s}+U^{\rm c}), \quad (10)$$

$$V^{\rm trip}(q) = -\frac{1}{2}U^{\rm s}\chi^{\rm s}(q)U^{\rm s}-\frac{1}{2}U^{\rm c}\chi^{\rm c}(q)U^{\rm c}+\frac{1}{2}(U^{\rm c}-U^{\rm s}). \quad (11)$$

The eigenvector $\psi(k)$ with the largest eigenvalue λ gives the most favorable superconducting pairing.

3. Result and discussion

3.1. Evolution of pairing symmetry with electron concentration

In our calculations, we have chosen the Hubbard interaction parameter $U=1.5$. We have verified that altering the value of Hubbard U does not result in qualitative changes in the main physical quantities (see Fig. A1 in Appendix A). Hence, this moderate level of interaction is sufficient for our theoretical analysis. Additionally, for the electron concentration of $n=4$, matching that of Sr_2RuO_4, we are able to reproduce the spin susceptibility with a peak at $(2\pi/3,2\pi/3)$ (Fig. A1), which is consistent with the experimental observations[64,65] and previous theoretical calculations.[66–73] Based on our method and model parameters, the leading superconducting pairing symmetry exhibits a $d_{x^2-y^2}$-wave structure (Fig. A1), aligning with prior theoretical findings on the spin-fluctuation-mediated pairing for a dominant incommensurate antiferromagnetic $(2\pi/3,2\pi/3)$ spin fluctuation.[71–74] However, the spin susceptibility also exhibits broad and prominent weights at low q and around (π,π). These features give rise to multiple competing superconducting pairing states and lead to variations in the most favorable state depending on the specific models utilized.[66–75] Thus, we can anticipate that the superconducting pairing states in our model will undergo changes in response to variations in particle concentration and interaction parameters.

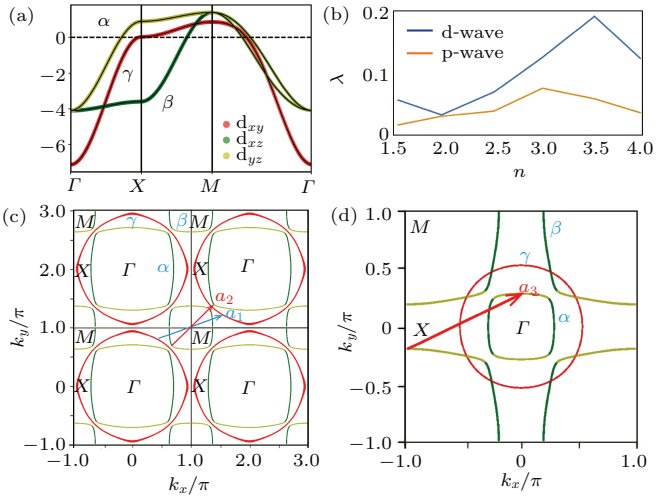


Fig. 1. (a) Energy band for $(t_1,t_2,t_3,t_4,\lambda,\Delta,\mu_0)=(1.0,0.395,1.25,0.125,0.1,0.2,1.35)$. (b) Evolutions of maximum eigenvalues of Eq. (9) in both the spin-singlet and spin-triplet channels for $J=0.25U$. (c) Fermi surface for $n=4$. (d) Fermi surface for $n=1.5$. The arrows in (c) and (d) represent the nesting wavevectors.

Let us begin by discussing the evolution of superconducting pairing symmetry with particle concentration. In this analysis, we fix the Hund's coupling to a moderate strength, i.e., $J=0.25U$. As depicted in Fig. 1(b), across the range of particle concentrations from $n=4$ to $n=1.5$, the maximum eigenvalue in the spin-singlet channel consistently surpasses that in the spin-triplet channel, suggesting a preference for the spin-singlet pairing symmetry for $J=0.25U$. To further investigate the pairing symmetries and understand their origins, we will examine the characteristics of the pairing function associated with the maximum eigenvalue. The pairing function matrix comprises nine (3×3) components. However, our numerical

results indicate that the non-diagonal elements can be considered negligible since their values are nearly zero.[76] Consequently, our discussion will primarily focus on the diagonal components of the pairing functions, namely, ψ_{11}, ψ_{22}, and ψ_{33}.

The pairing functions for two typical particle concentrations, namely, $n = 4$ and $n = 1.5$, are shown in Fig. 2. It can be observed that the superconducting pairing is orbital dependent. In the case of $n = 4$, the pairing strength of the d_{xy} orbital surpasses those of the other two orbitals by several times [Figs. 2(a)–2(c)]. This indicates that the superconducting pairing predominantly occurs in the quasi-two-dimensional d_{xy} orbital, which serves as the active orbital for superconductivity. Due to the absence of hybridization between d_{xy} and d_{xz}/d_{yz} orbitals, the pairing strengths on the passive orbitals (d_{xz} and d_{yz}) are considerably weaker. In contrast, for $n = 1.5$ [Figs. 2(d)–2(f)], the active orbitals shift to the d_{xz} and d_{yz} orbitals, which exhibit significantly larger pairing strengths compared to the d_{xy} orbital. For both particle concentrations, the pairing functions satisfy the d-wave symmetry, albeit with notable differences in their specific forms.

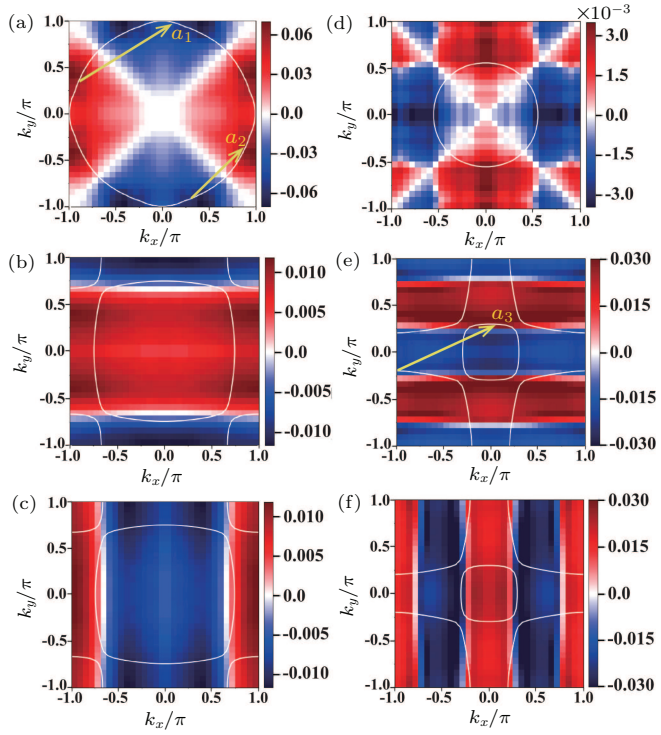


Fig. 2. Pairing functions for $n = 4$ (left panel) and $n = 1.5$ (right panel) with $J = 0.25U$. (a) and (d) ψ_{11}. (b) and (e) ψ_{22}. (c) and (f) ψ_{33}. The white lines in (a) and (d) are the Fermi surfaces of the γ band, and those in (b), (c), (e), and (f) are the Fermi surfaces of the α and β bands. The arrows in (a) and (e) connect two regions on the Fermi surface where the pairing functions change sign and exhibit significant intensity.

In the case of $J = 0.25U$, the spin susceptibilities are significantly larger than the charge susceptibilities.[76] Consequently, according to Eqs. (10) and (11), the pairing interactions are primarily influenced by spin fluctuations, and the spin-singlet pairing interaction is much stronger than the spin-triplet pairing interaction. This disparity explains the preference for spin-singlet superconductivity over spin-triplet superconductivity within the studied range of particle concentrations. To account for the origin of the pairing symmetry and its evolution with particle concentration, we will analyze the characteristics of spin susceptibilities. The distributions of the largest eigenvalues of the spin susceptibility tensor $\chi(\boldsymbol{k})$ are presented in Fig. A2. However, to analyze the origin of superconducting pairing symmetry, it is essential to consider the structure of each component. While the majority of the 81 components of $\chi(\boldsymbol{k})$ exhibit negligible values,[76] we can focus on the components with the highest intensities.

Figures 3(a)–3(c) display the spin susceptibility components $\chi^{\rm s}_{1111}$, $\chi^{\rm s}_{2222}$, and $\chi^{\rm s}_{2323}$ for $n = 4$. It is evident that the maximum value of $\chi^{\rm s}_{1111}$ is approximately 2–5 times larger than those of the other components, which is the main factor that makes the d_{xy} orbital the active orbital in superconducting pairing at this particle concentration. The characteristic wavevector of $\chi^{\rm s}_{1111}$ is located at $\boldsymbol{a}_1 = (\pi, \pi/2)$ [Fig. 3(a)], corresponding to the nesting wavevector $\boldsymbol{a}_1$ of the Fermi surface (FS) as shown in Fig. 1(c). For the superconducting pairing mainly mediated by spin fluctuations, if the spin susceptibility is prominent around a special wavevector $\boldsymbol{Q}$, the pairing scatterings will be dominated by $(\boldsymbol{k}, -\boldsymbol{k})$ to $(\boldsymbol{k}+\boldsymbol{Q}, -\boldsymbol{k}-\boldsymbol{Q})$ through exchanging the spin fluctuations around $\boldsymbol{Q}$ according to Eq. (9). Consequently, the pairing function $\psi(\boldsymbol{k})$ must satisfy the condition $\psi(\boldsymbol{k})\psi(\boldsymbol{k}+\boldsymbol{Q}) < 0$ in order to get the largest eigenvalue of Eq. (9), since the pairing interaction $V^{\rm sing}$ is positive. In our case here, the condition $\psi(\boldsymbol{k})\psi(\boldsymbol{k}+\boldsymbol{a}_1) < 0$ should be satisfied first, so the sign of the pairing function changes between the two parts of ψ_{11} connected by the wavevector $\boldsymbol{a}_1$, as shown in Fig. 2(a). In addition, the two parts connected by wavevector $\boldsymbol{a}_2$ in ψ_{11} also change sign [Fig. 2(a)]. However, there is no corresponding characteristic wavevector $\boldsymbol{a}_2$ in $\chi^{\rm s}_{1111}$. Instead, we can identify the corresponding wavevector in the spin susceptibility component $\chi^{\rm s}_{2222}$ [Fig. 3(b)]. Indeed, according to Eq. (10), the pairing interaction $V^{\rm sing}_{1111}$ for the d_{xy} orbital can be approximately written as

$$V^{\rm sing}_{1111} \approx \frac{3}{2}(U^2\chi^{\rm s}_{1111} + J^2\chi^{\rm s}_{2222} + J^2\chi^{\rm s}_{3333}), \tag{12}$$

where $\chi^{\rm s}_{3333}$ is just the result via rotating 90° of $\chi^{\rm s}_{2222}$. This implies that the pairing interaction of d_{xy} orbital also has contributions from spin fluctuations of the d_{xz} and d_{yz} orbitals. Therefore, the spin fluctuations in the passive orbitals d_{xz} and d_{yz} also affect the sign structure of ψ_{11} in the active orbital d_{xy}.

A notable change in the spin susceptibility occurs as the particle concentration decreases to $n = 1.5$, as illustrated in Figs. 3(d)–3(f). Specifically, the maximum values of $\chi^{\rm s}_{1111}$ are approximately one-fifth of that at $n = 4$, whereas the maximum value of $\chi^{\rm s}_{2222}$ remains almost unchanged. This can be

attributed to the fact that, at $n = 1.5$, the FS of d_{xy} orbital has already become a circle without a nesting structure [Fig. 1(d)], leading to a substantial reduction in the intensity of χ^{s}_{1111}. In contrast, the nesting properties of the FS of d_{xz} and d_{yz} orbitals remain nearly unchanged at different particle concentrations [Figs. 1(c) and 1(d)], explaining why the maximum values of χ^{s}_{2222} show only slight variations. At this lower particle concentration, the active orbitals for superconducting pairing have changed from d_{xy} to d_{xz} and d_{yz}, which can be confirmed by comparing the intensities of the pairing functions in different orbitals [Figs. 2(d)–2(f)]. In addition, the peak of χ^{s}_{2222} locates at $(\pi, \pi/2)$, labelled by $\boldsymbol{a}_3$ in Fig. 3(e). This peak originates from the nesting property of FS as shown in Fig. 1(d), and it also determines the sign structures of the pairing functions [Fig. 2(e)].

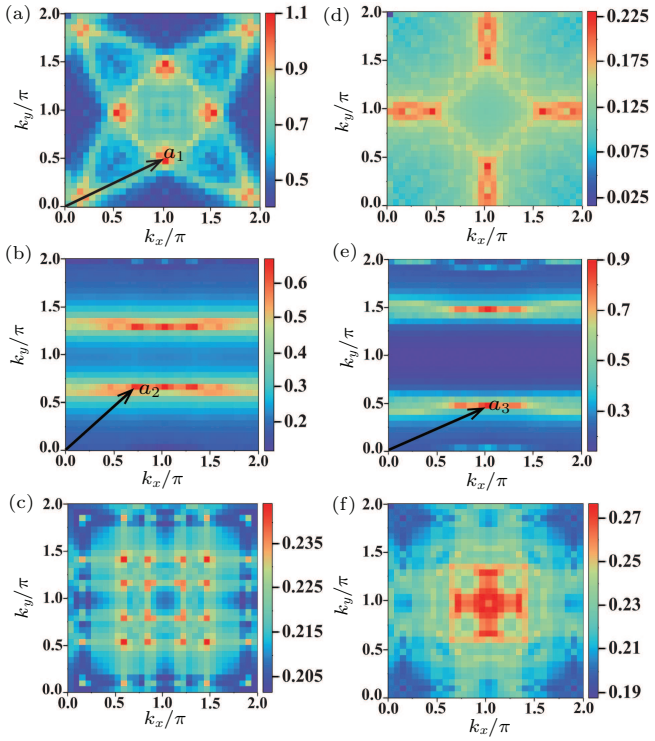


Fig. 3. Spin susceptibilities for $n = 4$ (left panel) and $n = 1.5$ (right panel) with $J = 0.25U$. (a) and (d) χ^{s}_{1111}. (b) and (e) χ^{s}_{2222}. (c) and (f) χ^{s}_{2323}. The arrows represent the characteristic wavevectors of the peaks.

Furthermore, Fig. 1(b) also exhibits a unique phenomenon: around $n = 2$, the maximum eigenvalue in the spin-singlet channel decreases significantly, forming a minimum and nearly degenerating with that in the spin-triplet channel. As shown in Figs. 4(a)–4(c), the dominant superconducting pairings are governed by the d_{xz} and d_{yz} orbitals at $n = 2$, so we will focus on the pairing functions ψ_{22} and ψ_{33}. This special phenomenon is still closely related to the characteristics of spin fluctuations. The main components of the spin susceptibility are shown in Figs. 4(d)–4(f). We find that the maximum value of χ^{s}_{2222} is considerably greater than that of χ^{s}_{1111}, which is consistent with that the d_{xz} and d_{yz} are the active orbitals for superconducting pairing. The peak values of χ^{s}_{2222} exhibit a stripe-like distribution with little variation in intensity, which reflects the one-dimensional feature of the d_{xz} orbital. Consequently, there exists a set of continuous characteristic wavevectors in χ^{s}_{2222}. In Fig. 4(e), we have plotted three representative wavevectors $\boldsymbol{a}_4$, $\boldsymbol{a}_5$, and $\boldsymbol{a}_6$. According to the aforementioned discussion, the pairing functions on the FS coming from the d_{xz} and d_{yz} orbitals should satisfy the sign-changing condition $\psi(\boldsymbol{k})\psi(\boldsymbol{k}+\boldsymbol{Q}) < 0$ as depicted in Fig. 4(b). However, the momenta connected by these wavevectors almost form $(\boldsymbol{k}, -\boldsymbol{k})$ pairs, which requires the pairing functions to satisfy $\psi(\boldsymbol{k}) = \psi(-\boldsymbol{k})$. This creates a contradiction between the sign structure required by the maximum eigenvalue and the fundamental requirements of singlet pairing. Due to the stripe feature of the peak distribution of the spin susceptibility, such contradictions occur at multiple continuous momentum points, resulting in a significant decrease in the eigenvalue in the spin-singlet channel. This also explains why the pairing intensities near the FS are almost zero [Figs. 4(b) and 4(c)]. Additionally, the inter-orbital sign structure of the pairing functions between the d_{xz} and d_{yz} orbitals [Figs. 4(b) and 4(c)] is determined by the peak of the inter-orbital spin susceptibility χ^{s}_{2323} located at $\boldsymbol{a}_7 = (\pi, \pi)$ [Fig. 4(f)]. Although the spin-singlet pairing is always more favorable than the spin-triplet pairing in the case of $J = 0.25U$, the near degeneracy of the two pairing types at $n = 2$ suggests that adjusting other model parameters is highly likely to enable the spin-triplet pairing.

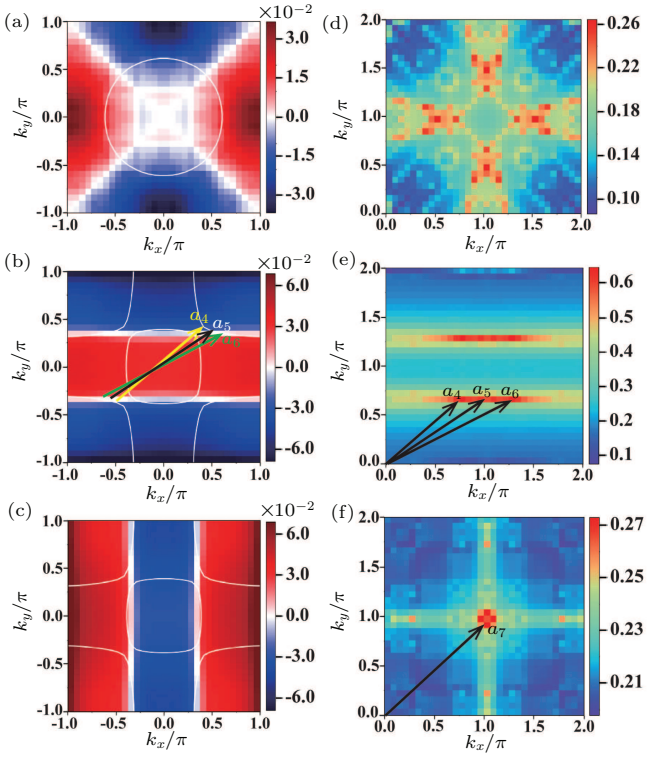


Fig. 4. Pairing functions (left panel) and spin susceptibilities (right panel) for $n = 2$ with $J = 0.25U$. (a) ψ_{11}, (b) ψ_{22}, (c) ψ_{33}, (d) χ^{s}_{1111}, (e) χ^{s}_{2222}, (f) χ^{s}_{2323}. The white lines indicate the Fermi surfaces. The arrows in (b) represent the nesting wavevectors, and the arrows in (e) and (f) represent the characteristic wavevectors of the peaks of the susceptibilities.

3.2. Impact of interactions on pairing symmetry

As mentioned above, there exists a significant competition between singlet and triplet pairings in the model under investigation. Therefore, by adjusting the interaction parameters, there is a potential for realizing spin-triplet superconductivity. Next, we will investigate how the variation of the Hund's coupling, namely J, influences the pairing symmetry. Figure 5(a) depicts the evolution of pairing symmetries with respect to J in both the spin-singlet and spin-triplet channels at $n = 2$. We find that the most favorable pairing symmetries in the spin-singlet and spin-triplet channels are d-wave and p-wave, respectively. Furthermore, we find that the spin-singlet superconductivity is more easily achieved with a large J, while the spin-triplet superconductivity is favored with a small J, with the phase transition between them occurring near $J = 0.25U$.

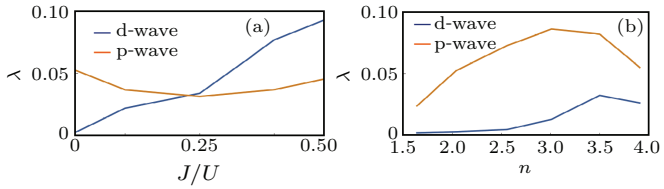


Fig. 5. (a) Evolutions of the maximum eigenvalues of Eq. (9) with J for $n = 2$. (b) Evolutions of the maximum eigenvalues of Eq. (9) with n for $J = 0$.

Due to the constrain of the relationship $U = U' + 2J$, a decrease of J corresponds to an increase of the interorbital Coulomb interaction U', which is directly associated with charge density fluctuations, so reducing J can enhance the role of charge fluctuations in driving superconducting pairing interactions. According to Eqs. (10) and (11), an increase in charge fluctuations will effectively reduce the spin-singlet pairing interactions but enhance the spin-triplet pairing interactions. To illustrate this more clearly, we present in Fig. 5(b) the evolution of pairing symmetry with the particle concentration, considering the extreme case of $J = 0$. Remarkably, the spin-triplet pairing emerges as the dominant pairing across the entire range of particle concentrations under studied. However, we find that although charge fluctuations do increase with the decrease of J, the peak of charge susceptibility remains consistently smaller than that of spin susceptibility.[76] Therefore, we will further analyze the contributions of spin fluctuations and charge fluctuations to pairing interactions through analytical calculations.

For the three-orbital model, both the spin and charge susceptibilities are represented by matrices of size 9×9, with 81 components, making analytical calculations quite cumbersome. To simplify the calculations, we will instead consider a two-orbital system that exhibits the same physics as the three-orbital system.[76] In order to further simplify the analysis, we focus on the limiting case of $J = 0$, accordingly $U' = U$. In this scenario, the interaction matrices U^{s} and U^{c} are

$$U^{\mathrm{s}} = \begin{pmatrix} U & 0 & 0 & 0 \\ 0 & U & 0 & 0 \\ 0 & 0 & U & 0 \\ 0 & 0 & 0 & U \end{pmatrix}, \tag{13}$$

$$U^{\mathrm{c}} = \begin{pmatrix} U & 0 & 0 & 2U \\ 0 & -U & 0 & 0 \\ 0 & 0 & -U & 0 \\ 2U & 0 & 0 & U \end{pmatrix}. \tag{14}$$

Furthermore, since many components of the spin and charge susceptibilities are nearly zero,[76] we only consider the most significant components, approximating the spin and charge susceptibilities as

$$\chi^{\mathrm{s}} = \begin{pmatrix} \chi^{\mathrm{s}}_{1111} & 0 & 0 & \chi^{\mathrm{s}}_{1122} \\ 0 & \chi^{\mathrm{s}}_{1212} & 0 & 0 \\ 0 & 0 & \chi^{\mathrm{s}}_{2121} & 0 \\ \chi^{\mathrm{s}}_{2211} & 0 & 0 & \chi^{\mathrm{s}}_{2222} \end{pmatrix}, \tag{15}$$

$$\chi^{\mathrm{c}} = \begin{pmatrix} \chi^{\mathrm{c}}_{1111} & 0 & 0 & \chi^{\mathrm{c}}_{1122} \\ 0 & \chi^{\mathrm{c}}_{1212} & 0 & 0 \\ 0 & 0 & \chi^{\mathrm{c}}_{2121} & 0 \\ \chi^{\mathrm{c}}_{2211} & 0 & 0 & \chi^{\mathrm{c}}_{2222} \end{pmatrix}. \tag{16}$$

By incorporating the above results into Eqs. (10) and (11), we express the effective pairing interactions in the spin-singlet and spin-triplet channels as

$$V^{\mathrm{sing}} = \frac{3}{2}\Gamma^{\mathrm{s}} - \frac{1}{2}\Gamma^{\mathrm{c}}, \tag{17}$$

$$V^{\mathrm{trip}} = -\frac{1}{2}\Gamma^{\mathrm{s}} - \frac{1}{2}\Gamma^{\mathrm{c}}, \tag{18}$$

where

$$\Gamma^{\mathrm{s}} = U^2 \begin{pmatrix} \chi^{\mathrm{s}}_{1111} & 0 & 0 & \chi^{\mathrm{s}}_{1122} \\ 0 & \chi^{\mathrm{s}}_{1212} & 0 & 0 \\ 0 & 0 & \chi^{\mathrm{s}}_{1212} & 0 \\ \chi^{\mathrm{s}}_{2211} & 0 & 0 & \chi^{\mathrm{s}}_{2222} \end{pmatrix}, \tag{19}$$

$$\Gamma^{\mathrm{c}} = U^2 \begin{pmatrix} \alpha+2(\beta+\gamma)+\delta & 0 & 0 & \beta+2(\alpha+\delta)+4\gamma \\ 0 & \eta & 0 & 0 \\ 0 & 0 & \eta & 0 \\ \gamma+2(\alpha+\delta)+4\beta & 0 & 0 & \delta+2(\beta+\gamma)+4\alpha \end{pmatrix}. \tag{20}$$

In the matrix Γ^{c}, the components α, β, γ, δ and η represent the charge susceptibility components χ^{c}_{1111}, χ^{c}_{1122}, χ^{c}_{2211}, χ^{c}_{2222} and χ^{c}_{1212}, respectively. It is evident that when the charge susceptibility components become comparable to, but not necessarily exceeding, the spin susceptibility components, the effective pairing interaction V^{trip} in the spin-triplet channel will surpass V^{sing} in the spin-singlet channel. Consequently, the spin-triplet superconductivity becomes more favorable than the spin-singlet superconductivity.

When the spin-triplet pairing predominates in this system, the most favorable pairing symmetry is consistently in the form of p-wave over the entire range of particle concentrations we investigated. Moreover, as shown in Fig. 6, for $n = 4$, the superconducting pairing is primarily driven by the d_{xy} orbital, while for $n = 1.5$, the active orbitals are d_{xz} and d_{yz}. Hence, similar to the case of $J = 0.25U$, the system

undergoes a transition from a quasi-two-dimensional orbital d_{xy}-dominated pairing state to a pairing state dominated by two quasi-one-dimensional orbitals d_{xz} and d_{yz}, as the particle concentration varies. For the p-wave pairings, the Eliashberg equation (9), a linear gap equation, yields two degenerate solutions with p_x and p_y symmetries, both belonging to the same irreducible representation of the system's symmetry group. In our calculations, the magnitude of each p-wave pairing and their relative phase cannot be determined, as they are determined by nonlinear effects. However, it is reasonable to expect that, in order to minimize the condensation energy, the system will spontaneously break the time-reversal symmetry and form a full-gaped $p_x + ip_y$ pairing.

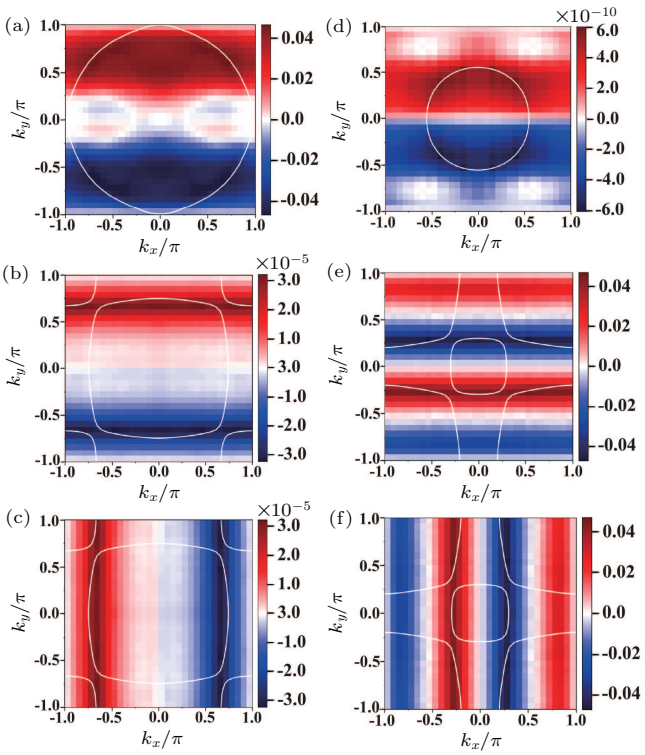


Fig. 6. Pairing functions for $n = 4$ (left panel) and $n = 1.5$ (right panel) with $J = 0$. (a) and (d) ψ_{11}. (b) and (e) ψ_{22}. (c) and (f) ψ_{33}.

4. Summary

In summary, we have employed the FLEX method to investigate the evolution of superconducting pairing symmetry in a t_{2g} three-orbital Hubbard model on the square lattice, considering various particle concentrations and interaction parameters. For moderate levels of Hund's coupling ($J = 0.25U$), spin fluctuations dominate the superconducting pairing, leading to a prevalent spin-singlet pairing with $d_{x^2-y^2}$-wave symmetry for all the particle concentrations that we have considered ($n = 1.5$–4). By reducing J to enhance charge fluctuations, we find that the superconducting pairing symmetry changes from spin-singlet $d_{x^2-y^2}$-wave to spin-triplet p-wave. These findings highlight the significant role of charge fluctuations in the superconducting mechanism of this three-orbital model. Moreover, regardless of whether it is a spin-singlet or spin-triplet pairing, we observe a shift of the active orbitals from the quasi-two-dimensional orbital d_{xy} to the quasi-one-dimensional orbitals d_{xz} and d_{yz} as the particle concentration varies from $n = 4$ to $n = 1.5$.

Appendix A: Results for different Hubbard interactions and distributions of the largest eigenvalues of χ^s

In this appendix, to demonstrate that changing the value of U within a certain range does not qualitatively affect our theoretical results, we present the spin susceptibilities and pairing functions for two representative values of U ($U = 1.0$ and $U = 2.0$) at $n = 4$ in Fig. A1. It is evident that the structures of the spin susceptibilities and pairing functions exhibit a high degree of consistency, with only minor variations in intensities. Therefore, the selection of U does not qualitatively impact our conclusions. We also observe that within the fluctuation exchange approximation, the superconducting pairing symmetry of our model at $n = 4$ is a singlet d-wave, which may be helpful for understanding the current experimental observations of singlet superconductivity in Sr_2RuO_4.

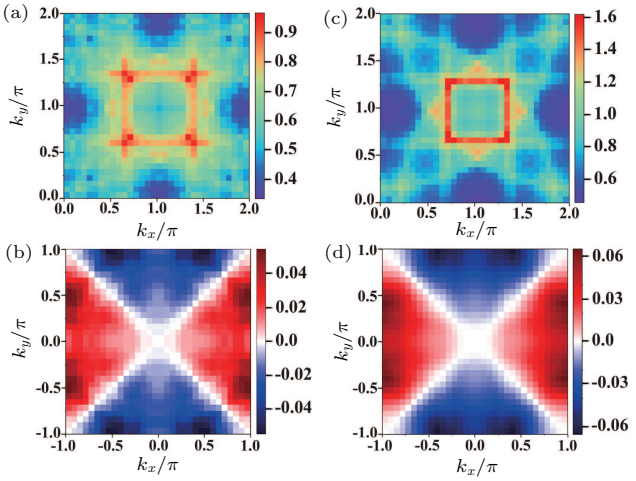


Fig. A1. Distributions of the largest eigenvalues of the spin susceptibilities $\chi(\boldsymbol{k})$ and pairing functions for $U = 1$ (left panel) and $U = 2$ (right panel) with the Hund's coupling $J = 0.25U$. (a) and (c) χ^s. (b) and (d) ψ_{11}.

The distributions of the largest eigenvalues of the susceptibility shown in Fig. A2 are related to Figs. 3 and 4 for $n = 1.5$ and $n = 2.0$, respectively.

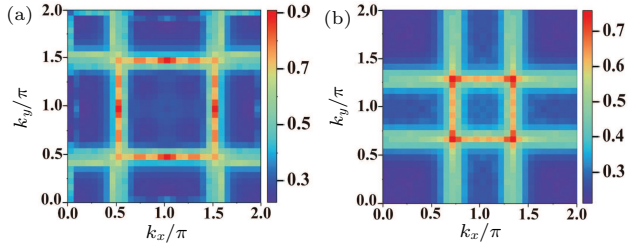


Fig. A2. Distribution of the largest eigenvalues of the spin susceptibility $\chi(\boldsymbol{k})$ for $U = 1.5$ and $J = 0.25U$. (a) $n = 1.5$. (b) $n = 2.0$.

Data availability statement

The data that support the findings of this study are openly available in Science Data Bank at https://doi.org/10.57760/sciencedb.j00113.00182.

Acknowledgements

Project supported by the National Key Research and Development Program of China (Grant No. 2021YFA1400400) and the National Natural Science Foundation of China (Grant Nos. 92165205, 12074175, and 12374137).

References

[1] Paglione J and Greene R L 2010 *Nat. Phys.* **6** 645
[2] Wang F and Lee D H 2011 *Science* **332** 200
[3] Dai P 2015 *Rev. Mod. Phys.* **87** 855
[4] Hosono H and Kuroki K 2015 *Physica C* **514** 399
[5] Fernandes R M, Chubukov A V and Schmalian J 2014 *Nat. Phys.* **10** 97
[6] Fernandes R M and Chubukov A V 2016 *Rep. Prog. Phys.* **80** 014503
[7] Yi M, Zhang Y, Shen Z X and Lu D 2017 *npj Quantum Materials* **2** 57
[8] Takimoto T 2000 *Phys. Rev. B* **62** R14641
[9] Mackenzie A P and Maeno Y 2003 *Rev. Mod. Phys.* **75** 657
[10] Bergemann C, Mackenzie A P, Julian S R, Forsythe D and Ohmichi E 2003 *Adv. Phys.* **52** 639
[11] Kallin C 2012 *Rep. Prog. Phys.* **75** 042501
[12] Maeno Y, Kittaka S, Nomura T, Yonezawa S and Ishida K 2012 *J. Phys. Soc. Jpn.* **81** 011009
[13] Mackenzie A P, Scaffidi T, Hicks C W and Maeno Y 2017 *npj Quantum Materials* **2** 40
[14] Leggett A J and Liu Y 2021 *J. Supercond. Nov. Magn.* **34** 1647
[15] Yu S L and Li J X 2012 *Phys. Rev. B* **85** 144402
[16] Kiesel M L, Platt C and Thomale R 2013 *Phys. Rev. Lett.* **110** 126405
[17] Wang W S, Li Z Z, Xiang Y Y and Wang Q H 2013 *Phys. Rev. B* **87** 115135
[18] Ortiz B R, Teicher S M L, *et al.* 2020 *Phys. Rev. Lett.* **125** 247002
[19] Zhao H, Li H, Ortiz B R, Teicher S M L, Park T, Ye M, Wang Z, Balents L, Wilson S D and Zeljkovic I 2021 *Nature* **599** 216
[20] Chen H, Yang H, Hu B, *et al.* 2021 *Nature* **599** 222
[21] Nie L, Sun K, Ma W, Song D, Zheng L, Liang Z, Wu P, Yu F, Li J, Shan M, Zhao D, Li S, Kang B, Wu Z, Zhou Y, Liu K, Xiang Z, Ying J, Wang Z, Wu T and Chen X 2022 *Nature* **604** 59
[22] Zheng L, Wu Z, Yang Y, Nie L, Shan M, Sun K, Song D, Yu F, Li J, Zhao D, Li S, Kang B, Zhou Y, Liu K, Xiang Z, Ying J, Wang Z, Wu T and Chen X 2022 *Nature* **611** 682
[23] Yin J X, Lian B and Hasan M Z 2022 *Nature* **612** 647
[24] Zhong Y, Liu J, Wu X, Guguchia Z, *et al.* 2023 *Nature* **617** 488
[25] Li D, Lee K, Wang B Y, Osada M, Crossley S, Lee H R, Cui Y, Hikita Y and Hwang H Y 2019 *Nature* **572** 624
[26] Li D, Wang B Y, Lee K, Harvey S P, Osada M, Goodge B H, Kourkoutis L F and Hwang H Y 2020 *Phys. Rev. Lett.* **125** 027001
[27] Gu Q, Li Y, Wan S, Li H, Guo W, Yang H, Li Q, Zhu X, Pan X, Nie Y and Wen H H 2020 *Nat. Commun.* **11** 6027
[28] Gu Q, Li Y, Wan S, Li H, Guo W, Yang H, Li Q, Zhu X, Pan X, Nie Y and Wen H H 2021 *Nat. Phys.* **17** 473
[29] Nomura Y and Arita R 2022 *Rep. Prog. Phys.* **85** 052501
[30] Gu Q and Wen H H 2022 *The Innovation* **3** 100202
[31] Sun H, Huo M, Hu X, Li J, Liu Z, Han Y, Tang L, Mao Z, Yang P, Wang B, Cheng J, Yao D X, Zhang G M and Wang M 2023 *Nature* **621** 493
[32] Singh Y and Gegenwart P 2010 *Phys. Rev. B* **82** 064412
[33] Liu X, Berlijn T, Yin W G, Ku W, Tsvelik A, Kim Y J, Gretarsson H, Singh Y, Gegenwart P and Hill J P 2011 *Phys. Rev. B* **83** 220403(R)
[34] Ye F, Chi S, Cao H, Chakoumakos B C, Fernandez-Baca J A, Custelcean R, Qi T F, Korneta O B and Cao G 2012 *Phys. Rev. B* **85** 180403(R)
[35] Hwan Chun S, Kim J W, Kim J, *et al.* 2015 *Nat. Phys.* **11** 462
[36] Chaloupka J, Jackeli G and Khaliullin G 2010 *Phys. Rev. Lett.* **105** 027204
[37] Singh Y, Manni S, Reuther J, Berlijn T, Thomale R, Ku W, Trebst S and Gegenwart P 2012 *Phys. Rev. Lett.* **108** 127203
[38] Sandilands L J, Tian Y, Plumb K W, Kim Y J and Burch K S 2015 *Phys. Rev. Lett.* **114** 147201
[39] Johnson R D, Williams S C, Haghighirad A A, Singleton J, Zapf V, Manuel P, Mazin I I, Li Y, Jeschke H O, Valentí R and Coldea R 2015 *Phys. Rev. B* **92** 235119
[40] Banerjee A, Bridges C A, Yan J Q, *et al.* 2016 *Nat. Mater.* **15** 733
[41] Sandilands L J, Tian Y, Reijnders A A, Kim H S, Plumb K W, Kim Y J, Kee H Y and Burch K S 2016 *Phys. Rev. B* **93** 075144
[42] Zhou X, Li H, Waugh J A, Parham S, Kim H S, Sears J A, Gomes A, Kee H Y, Kim Y J and Dessau D S 2016 *Phys. Rev. B* **94** 161106(R)
[43] Ran K, Wang J, Wang W, Dong Z Y, Ren X, Bao S, Li S, Ma Z, Gan Y, Zhang Y, Park J T, Deng G, Danilkin S, Yu S L, Li J X and Wen J 2017 *Phys. Rev. Lett.* **118** 107203
[44] Wang W, Dong Z Y, Yu S L and Li J X 2017 *Phys. Rev. B* **96** 115103
[45] Banerjee A, Yan J, Knolle J, Bridges C A, Stone M B, Lumsden M D, Mandrus D G, Tennant D A, Moessner R and Nagler S E 2017 *Science* **356** 1055
[46] Kasahara Y, Ohnishi T, Mizukami Y, Tanaka O, Ma S, Sugii K, Kurita N, Tanaka H, Nasu J, Motome Y, Shibauchi T and Matsuda Y 2018 *Nature* **559** 227
[47] Pavarini E and Mazin I I 2006 *Phys. Rev. B* **74** 035115
[48] Lee P A and Wen X G 2008 *Phys. Rev. B* **78** 144517
[49] Yu S L, Kang J and Li J X 2009 *Phys. Rev. B* **79** 064517
[50] Daghofer M, Nicholson A, Moreo A and Dagotto E 2010 *Phys. Rev. B* **81** 014511
[51] Fischer M H 2013 *New J. Phys.* **15** 073006
[52] Wang Q E and Zhang F C 2015 *Phys. Rev. B* **91** 214509
[53] Ghosh S and Singh A 2015 *New J. Phys.* **17** 063009
[54] Möckli D and de Mello E V L 2015 *EPL* **109** 17011
[55] Kanamori J 1963 *Prog. Theore. Phys.* **30** 275
[56] Bickers N E and Scalapino D J 1989 *Ann. Phys.* **193** 206
[57] Takimoto T, Hotta T and Ueda K 2004 *Phys. Rev. B* **69** 104504
[58] Dahm T, Tewordt L and Wermbter S 1994 *Phys. Rev. B* **49** 748
[59] Yan X Z and Ting C S 2006 *Phys. Rev. Lett.* **97** 067001
[60] Yao Z J, Li J X and Wang Z D 2009 *New J. Phys.* **11** 025009
[61] Onari S and Kontani H 2012 *Phys. Rev. B* **85** 134507
[62] Yu S L and Li J X 2013 *Chinese Phys. B* **22** 087411
[63] Wang H, Yu S L and Li J X 2015 *Phys. Rev. B* **91** 165138
[64] Sidis Y, Braden M, Bourges P, Hennion B, NishiZaki S, Maeno Y and Mori Y 1999 *Phys. Rev. Lett.* **83** 3320
[65] Braden M, Sidis Y, Bourges P, Pfeuty P, Kulda J, Mao Z and Maeno Y 2002 *Phys. Rev. B* **66** 064522
[66] Mazin I I and Singh D J 1999 *Phys. Rev. Lett.* **82** 4324
[67] Morr D K, Trautman P F and Graf M J 2001 *Phys. Rev. Lett.* **86** 5978
[68] Kuroki K, Ogata M, Arita R and Aoki H 2001 *Phys. Rev. B* **63** 060506(R)
[69] Eremin I, Manske D and Bennemann K H 2002 *Phys. Rev. B* **65** 220502(R)
[70] Boehnke L, Werner P and Lechermann F 2018 *Europhys. Lett.* **122** 57001
[71] Røer A T, Kreisel A, Müller M A, Hirschfeld P J, Eremin I M and Andersen B M 2020 *Phys. Rev. B* **102** 054506
[72] Røer A T, Scherer D D, Eremin I M, Hirschfeld P J and Andersen B M 2019 *Phys. Rev. Lett.* **123** 247001
[73] Gingras O, Nourafkan R, Tremblay A M S and Côté M 2019 *Phys. Rev. Lett.* **123** 217005
[74] Røer A T, Hirschfeld P J and Andersen B M 2021 *Phys. Rev. B* **104** 064507
[75] Wang Q H, Platt C, Yang Y, Honerkamp C, Zhang F C, Hanke W, Rice T M and Thomale R 2013 *Europhys. Lett.* **104** 17013
[76] See the supplemental material for detailed information on the components of the spin susceptibilities and pairing functions, as well as analytical results regarding pairing interactions in the case of $J = 0$ for the three-orbital model.